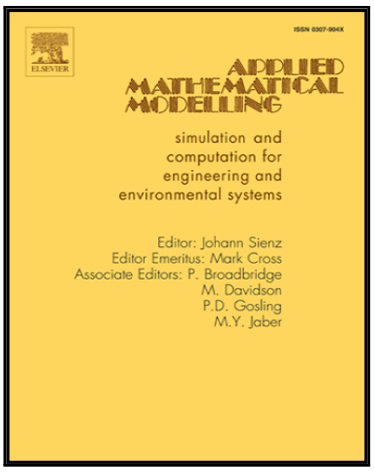

The influence of flow and thermal properties on injection pressure and cooling time prediction

Marton Huszar , Fawzi Belblidia , Sue Alston , Patrick Wlodarski , Cris Arnold , David Bould , Johann Sienz

PII: S0307-904X(16)30118-4
DOI: 10.1016/j.apm.2016.03.002
Reference: APM 11070

To appear in: *Applied Mathematical Modelling*

Received date: 20 May 2015
Revised date: 20 January 2016
Accepted date: 3 March 2016

Please cite this article as: Marton Huszar , Fawzi Belblidia , Sue Alston , Patrick Wlodarski , Cris Arnold , David Bould , Johann Sienz , The influence of flow and thermal properties on injection pressure and cooling time prediction, *Applied Mathematical Modelling* (2016), doi: 10.1016/j.apm.2016.03.002

Highlights

- An experimental and numerical case study for injection moulding is presented;
- The effect of material properties for mould filling/cooling stages was studied;
- True viscosity and no-flow temp. set to T_g yielded accurate pressure estimation;
- Thermal conductivity had negligible effect on pressure prediction;
- Molten state heat capacity and thermal cond. gave best estimate for cooling time.

The influence of flow and thermal properties on injection pressure and cooling time prediction

[*]Marton Huszar[1], Fawzi Belblidia[1], Sue Alston[1], Patrick Wlodarski[1], Cris Arnold[1], David Bould[1], Johann Sienz[1]

[1]College of Engineering (ASTUTE), Swansea University, Singleton Park, Swansea, SA2 8PP, UK
[*]Corresponding author: m.huszar@swansea.ac.uk

Abstract
Thermoplastic materials properties play an important role in mould filling and cooling analysis of injection moulding. Among the many, the melt`s viscosity, heat capacity and thermal conductivity may be the critical ones. An experimental and computational case study to determine the injection moulding window of a rectangular ABS plate is presented. When apparent viscosity of the material was adopted for cavity filling simulations, it was found that the computed injection pressure was overestimated in contrast to experimental data. Shear stress and rate corrections applied to apparent viscosity as well as the no-flow temperature (NFT) set to T_g (glass-transition temperature) helped to achieve more accurate pressure estimation. The heat capacity and thermal conductivity were both measured separately in solid and molten states and it was found that the best estimation for pressure and cooling time was achieved when molten state heat capacity was adopted for computation. The effect of thermal conductivity was negligible on pressure prediction, although the most accurate prediction for cooling time was attained when both molten state heat capacity and thermal conductivity were utilised.
Therefore, the quality of material data input was found to be a critical factor in achieving reliable flow properties. Accurate data available for mould and process design purposes may help to generate less production waste and save costs, making a step towards sustainable manufacturing.

Keywords: viscosity; heat capacity; thermal conductivity; injection pressure; cooling time; injection moulding simulation

1. Introduction

Injection moulding has been a common processing technique to produce plastic components. The cycle starts with the injection or filling phase, during which the injection screw moves forward carrying molten material to be injected into the mould cavity. When the cavity is nearly filled, the packing phase commences by forcing further molten material into the cavity to compensate for the shrinkage of the part. When the packing is finished and no pressure is further maintained, the cooling phase starts. Although heat loss from the melt may occur from the onset of the cycle, during this phase the remaining (largest amount of) heat from the material is removed until it is sufficiently solid to be ejected from the mould [1]. To explore the injection moulding feasibility of thermoplastic components, a processing window can be determined. In one approach, the injection pressure as a function of melt temperature and injection time may be recorded [2]. This injection pressure, utilised as a reference parameter, can be important for mould and process design purposes. In order to simulate the flow of the melt and determine the processing window, material properties are needed [1]. Among the many, viscosity, heat capacity and thermal conductivity may be the critical ones, which will ultimately influence the reliability of injection pressure and cooling time prediction.

The literature available regarding injection moulding and simulations is rich and it is beyond the interest of this paper to give a thorough insight into most of the work that has been undertaken. The purpose is to present to the reader a few examples regarding filling, packing and warpage analyses which were based on utilising computer simulation packages, such as Autodesk Moldflow (later on Moldflow).
In one study [3], the cavity fill balancing was emphasized as being an important criterion during filling analyses to improve the quality of the moulded parts. If an unbalanced flow pattern existed, that would lead to packing difficulties. Another work [4] pointed out that the appropriate selection of gate position would help to reduce the filling time and balance the moulded parts` temperature distribution. Others [5] studied a numerically obtained flow pattern of polypropylene at different injection velocities and compared the results with experimental data. It was found in some cases that the numerical analysis was not able to capture short-shot and jetting phenomena. Another paper [6] reported that filling difficulties could arise when moulding thin-walled components, as the frozen layer of the part would more rapidly develop with reduced thickness. To control the formation of the frozen layer, the appropriate selection of injection time and melt temperature would be necessary. Regarding packing analysis [7], it was reported that increased packing pressure would reduce the shrinkage of HDPE cups.

Specific to a warpage problem [8], it was shown that sustaining a longer cooling time and reduced melt temperature helped to improve the warpage of a box-like component.
Clearly, the correct interpretation of numerical results that were published in the aforementioned literature would not have been possible without the utilisation of accurate material properties. Regardless of whether additional packing and/or warpage analyses are performed (which require more complex material properties, such as pressure-volume-temperature data, coefficient of thermal expansion, mechanical properties, etc.) the very first task is to fill the mould cavity.
However, little information has been found that deals with the effect of the quantity and quality of material data input into injection moulding simulation packages.
For instance, it may happen that only apparent viscosity is available for a flow analysis. While other material properties, such as the heat capacity and thermal conductivity are not always readily available within that temperature range at which the plastic material is processed. This may be due to lack of data or having measurement difficulties at elevated temperatures. In this case, the designer may rely on literature or thermal properties available only in the solid state of the thermoplastic material. If inaccurate viscosity data or inappropriate magnitude of thermal properties is used for melt flow simulations, the computed injection pressure and cooling time might be incorrectly estimated which could be misleading for subsequent mould design analyses. In order to improve the efficiency of the design process it is therefore critical to utilise as accurate viscosity data as possible, and suitable values of specific heat capacity and thermal conductivity at various temperature ranges within the computational model.
An earlier work [2] pointed out the importance of corrections that can be applied to apparent viscosity. To extend this, in this paper not only the effects of the viscosity, but the NFT and the aforementioned two thermal properties of an amorphous ABS thermoplastic material with respect to a cavity filling analysis are considered. The details of experimental and numerical analysis are presented below.

2. Aim and methodology

The study was conducted to determine the mould processing window of a 3 mm thick rectangular plate with major dimensions [mm] depicted in Figure 1. It is important to note that the justification for selecting such a simple design was to eliminate the effect of geometrical complexity, thus concentrating solely on the effect of material properties.

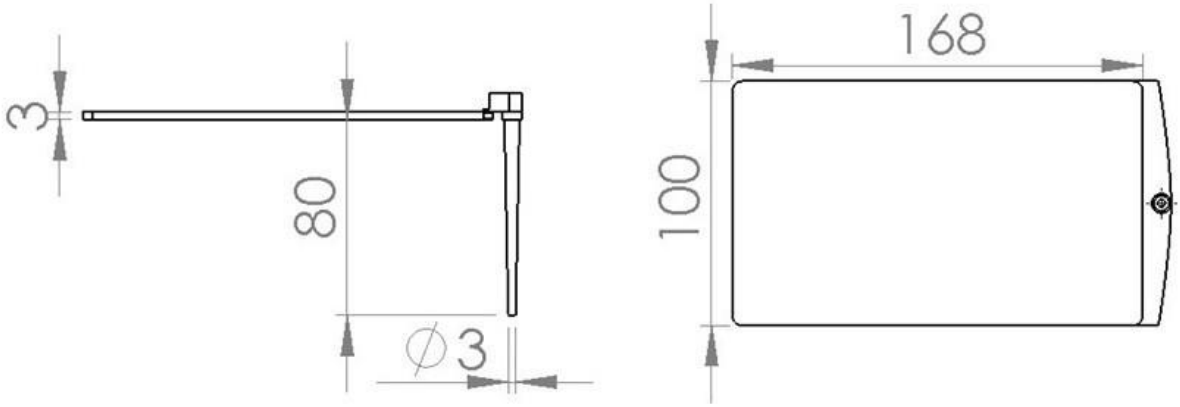

Figure 1. Major dimensions of the rectangular part

The experimental work utilised a Haitian HTF120X moulding machine and a generic grade of ABS thermoplastic. The processing window, i.e. the injection pressure limits were determined through the utilisation of a systematic factorial design consisting of three melt temperatures (220-, 240-, 260 °C) and three injection times (1-, 2-, 3 s). This was accomplished by reducing the hydraulic pressure of the machine until complete cavity filling was just achieved. The cooling time was set to 30 s and the cycle-average mould temperature of the Cu-mould was calculated based on the temperature readings of 12 thermocouples mounted in the mould. The values summarised in Table 1 were also applied in numerical simulations that will be introduced later. These values were applied as a mould temperature boundary condition imposed on the surface of mould. This was to ensure that uniform mould temperature was prescribed, eliminating transient effects.

Table 1. Cycle-average mould temperatures of the experimental work

Injection time [s]	Cycle-average mould temperatures [°C] at given melt temperatures [°C]			
	Melt temperature	220	240	260
1	Mould temperature	52	54	57
2		48	56	60
3		52	56	61

With respect to process improvement, the aim of the paper is twofold. The first is to highlight the importance of shear stress and rate corrections that can be applied to the apparent viscosity. The second is to explore the effects of the solid/molten state values of heat capacity and thermal conductivity regarding flow and thermal computation.

With reference to the viscosity of the ABS grade, it was measured on a Rosand twin-bore (ø 15.5 mm) capillary rheometer with dies of 20 x ø 1 mm and 0.1 x ø 1 mm. The shear rates were set in the range of 50-10000 1/s to account for the shear rates normally experienced during cavity filling. The resulting P pressures measured above the die which correspond to different Q volumetric flow rates can be used to calculate the τ (wall) shear stress and γ (wall) shear rate [9]. To obtain the apparent shear stress [Pa] of a Newtonian fluid, Equation 1 [10] can be used (where D and L are die diameter and length, respectively).

$$\tau_{apparent} = \frac{PD}{4L} \qquad \text{Equation 1}$$

Having known the volumetric flow rate of the melt, the apparent or Newtonian shear rate [1/s] can be determined. This correlation is described by Equation 2 [10].

$$\gamma_{apparent} = \frac{32Q}{\pi D^3} \qquad \text{Equation 2}$$

The apparent viscosity is then defined as $\eta_{apparent} = \tau_{apparent}/\gamma_{apparent}$ [Pa·s].
However, the possession of apparent viscosity is not yet satisfactory. During the rheology measurements, the capillary entrance effects cause deviations from the ideally developed pressure profile. Due to the change in cross section from the larger diameter of the barrel to the small one of the die, Equation 1 yields a shear stress that is larger than that in the fully developed flow region of the die [9] [11]. According to Bagley`s approach, this effect can be eliminated by conducting the measurement with (at least) two dies having the same diameter but different L/D ratio [10] [11]. Using Equation 3 [10], the true shear stress [Pa] based on Bagley`s approach can be obtained (where P_c is the pressure correction referring to different shear rates).

$$\tau_{true} = (P - P_c)\frac{D}{4L} \qquad \text{Equation 3}$$

In addition, polymer melts exhibit shear-thinning behaviour, hence the true shear rate is higher than the shear rate of Newtonian fluids [11]. To compensate this deviation, the Weissenberg-Rabinowitsch correction can be applied. Shown by Equation 4 [10], the true shear rate [1/s] is calculated by multiplying the apparent shear rate by the slope of apparent shear rate and true shear stress.

$$\gamma_{true} = \frac{\gamma_{apparent}}{4}\left(3 + \frac{d(\log \gamma_{apparent})}{d(\log \tau_{true})}\right) \qquad \text{Equation 4}$$

Then, the true viscosity is obtained by $\eta_{true} = \tau_{true}/\gamma_{true}$ [Pa·s].
As explained in Equation 5, both the apparent and true viscosities were data fitted separately into the Cross-(William-Landel-Ferry, WLF) viscosity model based on the minimisation of the root-mean-square deviation (RMSD) [12] between the fitted and measured data.

$$RMSD = \sqrt{\frac{1}{y}\sum_{i=1}^{y}\left(\frac{\eta_m^i - \eta_f^i}{\eta_m^i}\right)^2} \qquad \text{Equation 5}$$

Where: y is the number of data points, η_m and η_f are the measured and fitted viscosity respectively.

In Equation 6, the Cross-model [1] has the form of:

$$\eta = \frac{\eta_0}{1+\left(\frac{\eta_0 \gamma}{\tau^*}\right)^{1-n}} \qquad \text{Equation 6}$$

The correlation above is capable of treating the viscosity in both the Newtonian-plateau and shear-thinning behaviour of the melt. The zero shear-rate viscosity, η_0 [Pa·s] is predicted at γ~0 1/s. τ^* [Pa] is the critical shear-stress that is needed to transform the melt flow from the Newtonian to the shear-thinning or power-law behaviour; while n is the measure of degree of the shear-thinning behaviour [1].

To account for the change in temperature of the melt, a time-temperature shift factor formulated by WLF [1] is coupled with Equation 6. The correlation in Equation 7 treats the zero shear-rate viscosity, η_0 as a function of D_1 [Pa·s], A_1 [-], A_2 [K] material constants, T_g [K] (the measurement details will be presented shortly) and corresponding T melt processing temperature [K]. Regarding data fitting, the parameters of n, τ^*, D_1 and A_1 were varied.

$$\eta_0 = D_1 \exp\left(\frac{-A_1(T-T_g)}{A_2+(T-T_g)}\right) \qquad \text{Equation 7}$$

After obtaining the Cross-WLF models coefficients of apparent and true viscosities, these were imported into Moldflow to be able to perform 3D non-isothermal numerical simulations using the Navier-Stokes solver based on the following governing Equations 8-12 [13] for mass, momentum and energy respectively (further information regarding the solver may be found in [1]).

$$\text{Mass:} \quad \frac{\partial \rho}{\partial t} + \frac{\partial(\rho u)}{\partial x} + \frac{\partial(\rho v)}{\partial y} + \frac{\partial(\rho w)}{\partial z} = 0 \qquad \text{Equation 8}$$

$$\text{Momentum:} \quad \rho\left(\frac{\partial u}{\partial t} + u\frac{\partial u}{\partial x} + v\frac{\partial u}{\partial y} + w\frac{\partial u}{\partial z}\right) = -\frac{\partial p}{\partial x} + \eta\left(\frac{\partial^2 u}{\partial x^2} + \frac{\partial^2 u}{\partial y^2} + \frac{\partial^2 u}{\partial z^2}\right) + \rho g_x \qquad \text{Equation 9}$$

$$\rho\left(\frac{\partial v}{\partial t} + u\frac{\partial v}{\partial x} + v\frac{\partial v}{\partial y} + w\frac{\partial v}{\partial z}\right) = -\frac{\partial p}{\partial y} + \eta\left(\frac{\partial^2 v}{\partial x^2} + \frac{\partial^2 v}{\partial y^2} + \frac{\partial^2 v}{\partial z^2}\right) + \rho g_y \qquad \text{Equation 10}$$

$$\rho\left(\frac{\partial w}{\partial t} + u\frac{\partial w}{\partial x} + v\frac{\partial w}{\partial y} + w\frac{\partial w}{\partial z}\right) = -\frac{\partial p}{\partial z} + \eta\left(\frac{\partial^2 w}{\partial x^2} + \frac{\partial^2 w}{\partial y^2} + \frac{\partial^2 w}{\partial z^2}\right) + \rho g_z \qquad \text{Equation 11}$$

$$\text{Energy:} \quad \rho C_p\left(\frac{\partial T}{\partial t} + u\frac{\partial T}{\partial x} + v\frac{\partial T}{\partial y} + w\frac{\partial T}{\partial z}\right) = k\left(\frac{\partial^2 T}{\partial x^2} + \frac{\partial^2 T}{\partial y^2} + \frac{\partial^2 T}{\partial z^2}\right) + \eta\gamma^2 \qquad \text{Equation 12}$$

Where ρ is the density, u, v and w are velocity vectors, x, y and z are Cartesian coordinates, t is the time, g is the gravitational force, T is the temperature, C_p is the heat capacity, k is the thermal conductivity. γ is the shear-rate, as defined by Equation 13 [13]:

$$\gamma = \sqrt{\left(\frac{\partial u}{\partial x}\right)^2 + \left(\frac{\partial v}{\partial y}\right)^2 + \left(\frac{\partial w}{\partial z}\right)^2} \qquad \text{Equation 13}$$

With initial conditions, defined by Equation 14-15 [13]:

$$\text{At mould wall:} \quad u, v, w = 0; T = T_{wall} \qquad \text{Equation 14}$$

$$\text{At part centre-line:} \quad \frac{\partial u}{\partial z} = \frac{\partial v}{\partial z} = \frac{\partial w}{\partial z} = \frac{\partial T}{\partial z} = 0 \qquad \text{Equation 15}$$

And boundary conditions, set out by Equation 16-18 [13]:

At flow front: $p = 0$ Equation 16

At inlet: $p = p(x, y, z, t)$ Equation 17

At mould wall in normal direction: $\frac{\partial p}{\partial n} = 0$ Equation 18

To ensure that computational discrepancies due to mesh were attenuated, a mesh convergence study using the injection pressure as a reference parameter was conducted to select the most suitable (3D tetrahedral unstructured) mesh to be employed in the study. As shown in Figure 2, the convergence was reached at ~1055000 no. of elements, therefore this mesh was selected for numerical analyses.

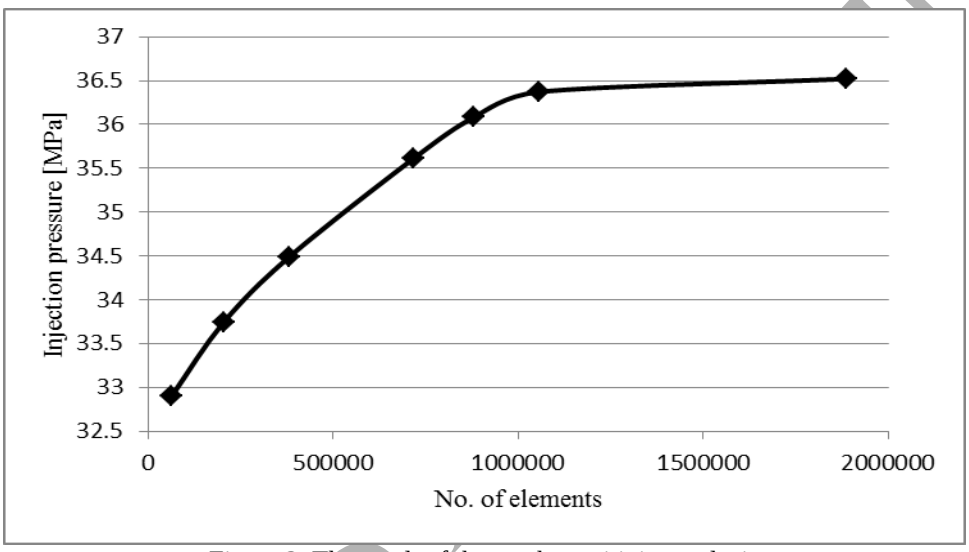

Figure 2. The result of the mesh sensitivity analysis

Regarding the thermal properties of the ABS grade, the onset of the T_g was determined (T_g ~ 106 °C) by a Perkin Elmer DSC apparatus in accordance with ISO 11357. The heat capacity was also measured in the solid and molten states in the range of 60-100 and 210-270 °C (with 10 °C increments in both states), respectively. By definition, the heat capacity is the heat energy required to raise the temperature of the material. It also expresses how much energy is stored in the material at a given temperature [1].

At this point it is worth mentioning the concept of no-flow temperature (NFT) that is used by Moldflow to capture the formation of the frozen layer. This parameter is used for simplifying the flow calculation and overcoming the lack of accuracy of the viscosity model in low-temperature regions (i.e. temperature close to solidification) [14]. This material property may be measured by conducting flow experiments and recording the temperature below which the material will cease flowing. For semi-crystalline grades, the NFT may be estimated to be 10-80 °C below the melting temperature. By restricting the discussion to amorphous materials, it can be valid that the NFT≥T_g [12]. In one study [15] however, it was assumed that NFT=T_g+30 °C.

In this work, to study the effect of NFT, a sensitivity analysis for injection pressure prediction based on NFT=T_g, NFT=T_g+15 °C and NFT=T_g+30 °C was also performed.

The α thermal diffusivity [m^2/s] was measured by a Netzsch LFA 457 laser flash device in the solid state of the material at 60-, 80-, 100 °C as well as in the molten state at 220-, 240-, 260 °C. The thermal conductivity was calculated from the thermal diffusivity ($\alpha=k/\rho C_p$), based on the corresponding solid/molten state heat capacity and density (1021.35 kg/m^3 and 935.21 kg/m^3 respectively, obtained from Moldflow`s database [16]).

The justification for selecting exclusively the solid/molten state data was based on the assumption that within these two regimes the thermal properties do not vary significantly. Hence, it is believed that the utilisation of this two-level approach will allow one to have sufficient information regarding the effect of both thermal properties. The average values of heat capacity and thermal conductivity together with the standard deviations in round brackets are summarised in Table 2 (the thermal conductivity values for semi-crystalline grades compared to amorphous ones may be significantly different. Upon reaching the melting temperature, the crystalline phase dissolves, resulting in lower thermal conductivity in the molten state [17]).

Table 2. Heat capacity and thermal conductivity of the ABS grade

Thermal property	Solid state	Molten state
C_p [J/kgK]	687 (8)	1697 (24)
k [W/mK]	0.11 (0.012)	0.15 (0.007)

Equation 19 [1] may be used to define thermal conductivity, which is a proportionality constant referring to how quickly the heat can be drawn from the melt.

$$\frac{\Delta Q}{\Delta t} = kA\frac{\Delta T}{\Delta x} \qquad \text{Equation 19}$$

Where: ΔQ is the heat flow across the cross-section area A, through thickness Δx (of the part) in time Δt. ΔT refers to the temperature difference between the hot (melt) and cold (mould) surfaces and k is the thermal conductivity.
The heat capacity and thermal conductivity have important implications during heat transfer in injection moulding. Conduction out of the melt and shear heating caused by the shear-flow of the melt occur [1]. Using Equation 20 [18], the overall heat transfer during filling/packing/cooling stages is governed by the transient 3D Poisson equation:

$$\rho c_p \frac{\partial T}{\partial t} = k\left(\frac{\partial^2 T}{\partial x^2} + \frac{\partial^2 T}{\partial y^2} + \frac{\partial^2 T}{\partial z^2}\right) \qquad \text{Equation 20}$$

Where, t is the time, T is the temperature and x, y, z are Cartesian coordinates respectively.
In this paper, three analyses will be presented. In the first one, the melt/mould temperatures and injection times were set in Moldflow identical to those that were set during the experimental work, as summarised in Table 1. Since the material is molten during the filling stage, the heat capacity and thermal conductivity obtained in the molten state (Table 2) were adopted. Then, the experimental and numerically predicted injection pressure values were contrasted in light of apparent and true viscosities. In addition, the effect of different NFT values was also considered. The second analysis utilised the heat capacity and thermal conductivity obtained both in solid and molten states. These were combined into a systematic factorial matrix to explore their effects regarding injection pressure, clamp force (which is required to keep the mould halves closed during the injection cycle) and part temperature. By using the same factorial matrix as mentioned before, the third analysis investigated the effects of the aforementioned thermal properties on cooling time prediction. Last but not least, a mould design consideration, i.e. definition for gate dimensions will be presented to link the results to sustainable injection moulding.

3. Results and discussion

3.1. Effect of viscosity on injection pressure prediction

With respect to data fitting, the calculated Cross-WLF viscosity coefficients are presented in Table 3. After performing the corrections according to Equation 3-4, it became clear that, $\tau_{apparent} > \tau_{true}$ and $\gamma_{apparent} < \gamma_{true}$, therefore $\eta_{apparent} > \eta_{true}$. Also, the degree of shear-thinning behaviour $n_{apparent} > n_{true}$ yielded that the critical shear-stress was $\tau^*_{apparent} < \tau^*_{true}$.

Table 3. Model coefficients of fitted viscosity data

Cross-WLF model coefficients	Viscosity of the ABS grade	
	Apparent	*True*
n [-]	0.30	0.23
τ* [Pa]	55814	99253
D_1 [Pa·s]	6.30E+10	1.37E+11
A_1 [-]	22.80	24.81
A_2 [K]	51.6	51.6
T_g [K]	379.15	379.15
RMSD	0.11	0.06

For the sake of further explanation, the viscosity considered at 220 °C is illustrated in Figure 3. References are given to η_0, τ^* and n as well as to apparent/true and fitted/measured viscosity data points (the measured viscosity spans the 50-10000 1/s shear rate regime).

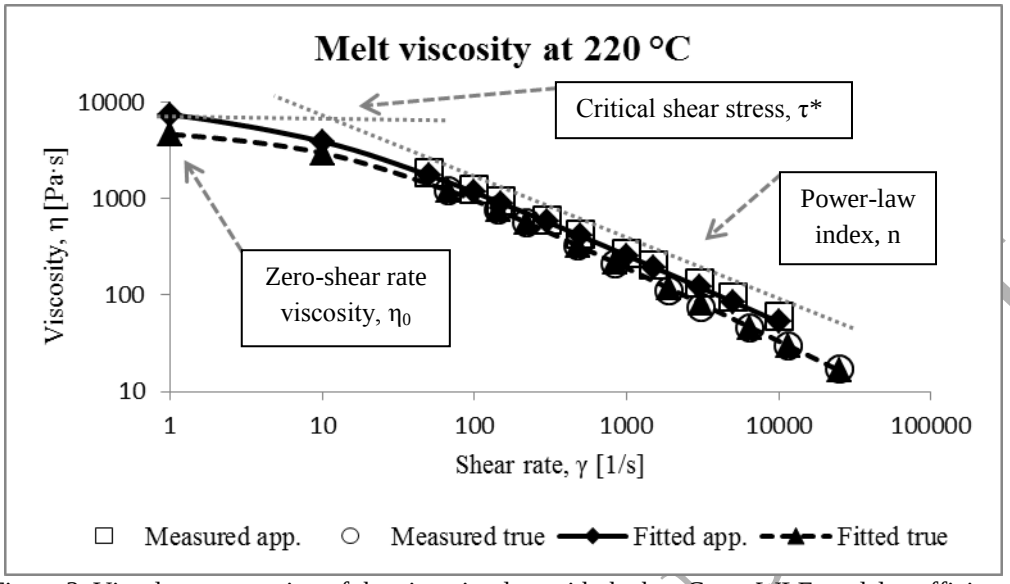

Figure 3. Visual representation of the viscosity data with the key Cross-WLF model coefficients

By considering the NFT=T_g approach, it was found that the apparent viscosity on average was 46% higher than the true viscosity. Similar findings were reported in literature (63%) [19], however with differences being dependent on the power-law index.

The figures in Table 4 show that working with the apparent viscosity led to overestimations from experimentally obtained (measured) injection pressures. It is noticeable that the overestimation of pressure is attenuated by utilising the true viscosity for simulations. It can be claimed that more accurate injection pressure prediction can be achieved if the true viscosity is applied. Deviations however, are still present, although these become lower compared to the results if apparent viscosity is considered. The average overestimation of injection pressure was 15 % for the apparent viscosity and 7 % for the true viscosity, respectively. In some cases, larger deviations (~20-30 %) were identified.

In one study [14] it was stated that the change of NFT did not appreciably affect the injection pressure. However, in this work under present conditions it was found that the pressure values obtained by true viscosity with NFT=T_g, NFT=T_g+15 °C (data not shown) and NFT=T_g+30 °C were overestimated on average by 7%, 12% and 18% relative to the experimental data. It may be stated that the magnitude of pressure overestimation linearly increases with the rise in NFT. The overestimation of pressure with NFT=T_g+30 °C is larger than the one calculated when apparent viscosity was used for computation. Since the solidification of the melt commences at an elevated (T_g+30 °C) temperature, more frozen volume will develop, giving a rise in injection pressure. The computation with NFT=T_g+30 °C is not favourable since it returns greatly overestimated injection pressures. Therefore, for all forthcoming analyses the true viscosity with NFT=T_g was considered.

Table 4. Differences between numerical and experimental injection pressure

Viscosity utilised for numerical analyses	(Numerical/**experimental data** [MPa]) and difference relative to experimental ones [%]			
	Injection time [s]	Melt temperature [°C]		
		220	240	260
Apparent *(NFT=T_g)*	1	(99/**90**) 10	(82/**79**) 3	(67/**64**) 4
	2	(92/**68**) 35	(71/**56**) 27	(57/**49**) 17
	3	(87/**78**) 12	(68/**58**) 17	(53/**48**) 11
True *(NFT=T_g)*	1	(91/**90**) 1	(75/**79**) -5	(61/**64**) -5
	2	(87/**68**) 27	(68/**56**) 21	(53/**49**) 8
	3	(81/**78**) 4	(63/**58**) 9	(49/**48**) 3

True *(NFT=T_g+30°C)*	1	(99/**90**) 10	(82/**79**) 3	(68/**64**) 6
	2	(93/**68**) 37	(74/**56**) 32	(60/**49**) 23
	3	(90/**78**) 15	(70/**58**) 21	(55/**48**) 15

3.2. Effect of thermal properties on injection pressure, clamp force and part temperature

This computation utilised the solid/molten state heat capacity and thermal conductivity values combined into a two-level factorial matrix. To contrast the effects of thermal properties regarding numerically predicted injection pressure, the pressure value of 90 MPa obtained by experimentation at 220 °C melt-, 52 °C mould temperature and 1 s injection time (Table 4) was used as a reference parameter.

It is shown in Table 5 that variations among numerically predicted injection pressure and clamp force after the cavity filling were observed. The clamp force, exerted by the clamping unit, is required to keep the mould halves closed during the injection cycle which is in direct relationship with the injection pressure. In a simple approach, it may be estimated by multiplying the part`s projected area with the injection pressure (or cavity pressure, if available). To have a better understanding concerning the variations in computed injection pressure, the part temperature should be assessed. Those values were investigated at the strip gate/part junction area after the filling cycle as illustrated in Figure 4 (the outer surface of the part indicates the 52 °C mould temperature to which reference was given earlier). This is the position where the solid part is practically detached from the gating system after ejection and to which reference will be given shortly regarding cooling time prediction.

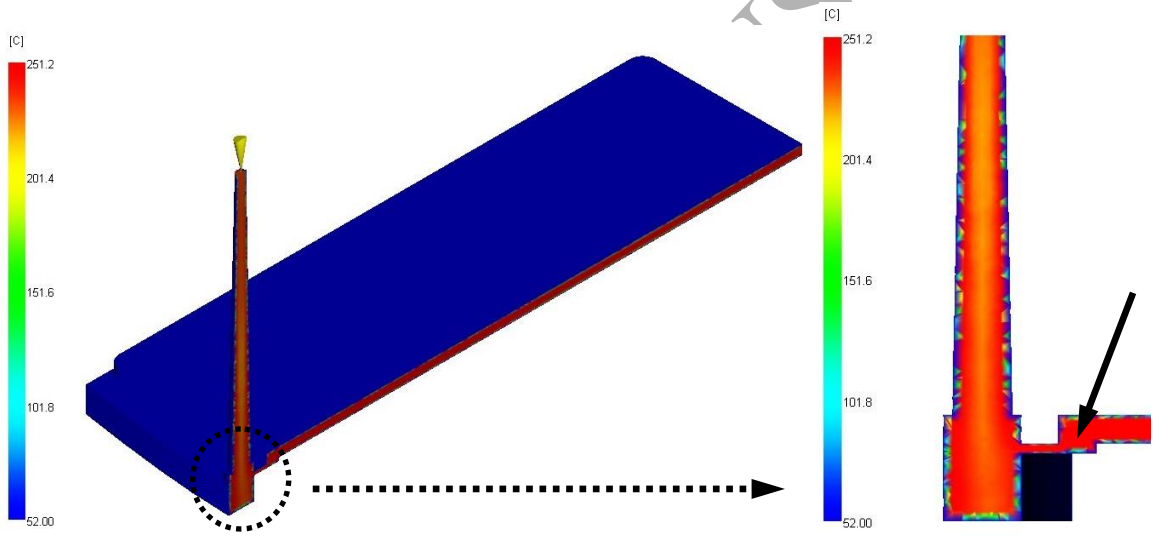

Figure 4. Cross-sectioned part temperature plot and strip gate/part junction query position for temperature

It can be noticed that the part temperature increased in all four scenarios (relative to the pre-set 220 °C), with magnitudes depending on whether molten or solid state specific heat capacity was utilised. The rise in part temperature is a function of two important conditions and has direct implication towards pressure and consequently clamp force prediction. In a shear-driven flow, shear-heat is generated, which is the function of viscosity and shear rate [1]. The experimental and numerical analysis utilised a relatively fast 1 s injection time (~59 cm^3/s flow rate) allowing shear-heat to be generated. The second condition is the specific heat capacity of the material. Lower heat capacity means that less energy is needed to give rise in the temperature. Consequently, for a fast injection rate, more shear-heat is generated. If the solid state heat capacity is utilised for numerical analysis, overestimated part temperature by ~12 % will be recorded in contrast to the temperature when molten state heat capacity is considered. Clearly, if the temperature is overestimated, the viscosity gets unrealistically reduced, resulting in lower injection pressure and clamp force. Hence, the use of solid state heat capacity for computation is not favourable, as it returns greatly underestimated pressures. Numerically, the differences are ~16 % underestimation for solid-, and ~14 % for molten state thermal conductivity.

If molten state heat capacity and solid state thermal conductivity are utilised for computation, only ~1 % underestimation of pressure was recorded. Similarly, ~1 % overestimation was computed if the molten state thermal conductivity would be used. This suggests that the thermal conductivity has a minor effect on the outcome of pressure calculation, provided molten state heat capacity is used. In this scenario, the predicted clamp forces are almost identical, as well as the part temperature values remained unchanged.

Table 5. The impact of thermal properties on pressure, clamp force and part temperature

Thermal properties and their levels, C_p [J/kgK], k [W/mK]		(Numerical/**experimental injection pressure** [MPa]) and difference relative to experimental ones [%]	Clamp force (numerical) [t]	Strip gate/part junction temperature (numerical) [°C]
C_p, 687 (solid)	k, 0.11 (solid)	(75/**90**) -16	~30	~279
C_p, 687 (solid)	k, 0.15 (molten)	(77/**90**) -14	~33	~281
C_p, 1697 (molten)	k, 0.11 (solid)	(89/**90**) -1	~36	~249
C_p, 1697 (molten)	k, 0.15 (molten)	(91/**90**) 1	~37	~249

It can be stated that the utilisation of molten state specific heat capacity generates the most realistic pressure prediction, irrespective of the levels of thermal conductivity (due to $k_{solid} \sim k_{melt}$). In this scenario, a sensible amount of shear heat is generated; hence the viscosity and pressure are more reliably approximated.
To give a physical insight into what the pressure difference may represent in reality, two samples, one from the fully filled cavity and one from a shorted cavity (incomplete filling) were collected, both are depicted in Figure 5. The complete cavity filling was achieved at 85 MPa injection pressure and the shorted one at 83 MPa respectively. Other experimental conditions include the melt temperature of 210 °C and injection time of 3 s.

Figure 5. A complete cavity filling (left) and a shorted cavity (right)

3.3. Effect of thermal properties on cooling time prediction

The melt may lose heat from the onset of the injection cycle by magnitudes depending on process conditions, however the largest amount of heat is removed during the cooling stage. It should be noted that there is a very complex relationship among part/mould design and processing related variables, hence the determination of true cooling time at which a part will solidify has been a great challenge. Since the cooling time is the longest time interval of the whole injection cycle [20], the determination of how the thermal material properties influence this duration is of great importance towards attaining the best estimation.
Besides the injection pressure, clamp force and part temperature as discussed earlier, numerical approximations for the cooling time - referring to the time required to reach a predefined, 93 °C ejection temperature [16] - were also extracted after the filling analyses were finished.
As illustrated in Figure 6, the numerical cooling time values were investigated at three different areas of the geometry, corresponding to the bottom of the (tapered) cylindrical runner, strip gate as well as at the strip gate/part junction areas.

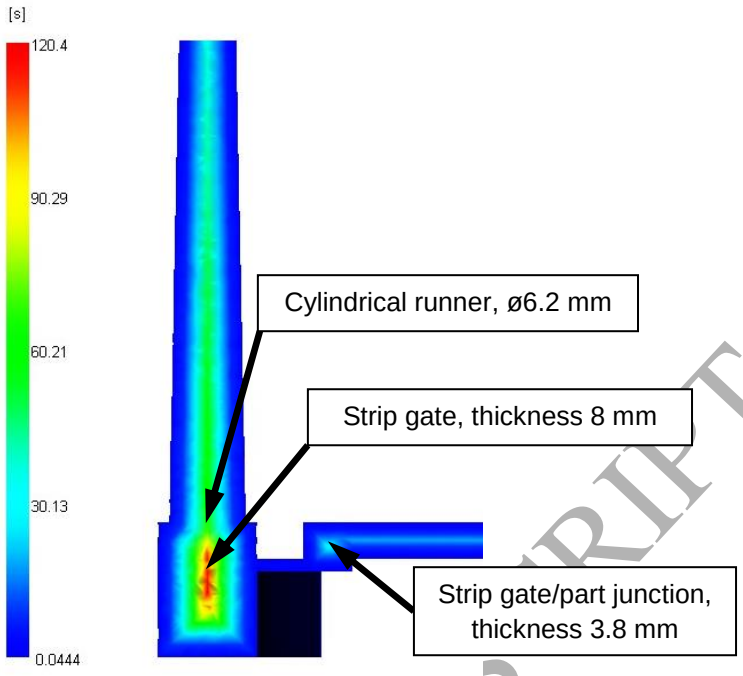

Figure 6. Query positions for cooling time values

In Figure 6 one may notice a "hot-spot" on the contour plot. Since the largest cross-section is at the strip gate, the computed cooling time is the longest. In theory, for the calculation of cooling time the largest cross-section should be considered. However, this is often not the case in reality. The explanation is that the whole runner system need not to be as rigid as the part being de-moulded so the necessary cooling time may be adjusted to the maximum part thickness [21].

For present geometry the maximum part thickness is represented at the strip gate/part junction, where the solid part is practically detached from the gating system after ejection. Hence, an analytical prediction for cooling time at the strip gate/part junction based on Equation 21 [22] was also adopted. This approach considers the cooling time to be the interval until the end of the injection stage when the centreline (half cross-section) of the part temperature at the maximum part thickness reaches the predefined ejection temperature.

$$t_c = \frac{h^2}{\alpha \pi^2} \ln\left[\frac{4}{\pi}\left(\frac{T_m - T_w}{T_e - T_w}\right)\right] \qquad \text{Equation 21}$$

Where, t_c is the cooling time, h is the local part thickness, α is the thermal diffusivity of the melt, T_m-, T_w and T_e are the melt-, mould wall surface and ejection temperatures, respectively.
The analytical estimation of cooling time at the aforementioned area with the 3.8 mm local thickness, 52 and 93 °C mould and ejection temperatures were utilised. The melt temperatures defined in Table 5 as well as a reference density (average of solid and molten state densities) of 978.28 kg/m^3 were adopted.

The cooling times obtained by numerical and analytical approaches are summarised in Table 6. For convenience, the values for the cylindrical runner and strip gate are also included, however the assessment was based on the cooling times at the strip/gate junction.
Relative to the experimentally set 30 s cooling time, shorter cooling times were predicted numerically by using the solid state heat capacity. Since the ability of the material to retain the heat in solid state is poorer, hence shorter cooling times were predicted by magnitudes depending on whether solid or molten state thermal conductivities were utilised. Solid state heat capacity coupled with solid and molten state thermal conductivity underestimated the cooling time by 38 % and 54 % respectively.
Better approximations were achieved when the molten state heat capacity was adopted. When this was coupled with solid and molten state thermal conductivity a 38 % overestimation and 0 % deviation were predicted relative to the experimental cooling time.

Table 6. The impact of thermal properties on cooling time

Thermal properties and their levels, C_p [J/kgK], k [W/mK]		(Numerical/**experimental cooling time** [s]) and difference relative to experimental ones [%]			Analytical cooling time [s]
		Cylindrical runner	Strip gate	Strip gate/part junction	Strip gate/part junction
C_p, 687 (solid)	k, 0.11 (solid)	~38	~71	(~19/**30**) -38	~17
C_p, 687 (solid)	k, 0.15 (molten)	~27	~52	(~14/**30**) -54	~13
C_p, 1697 (molten)	k, 0.11 (solid)	~93	~164	(~41/**30**) 38	~40
C_p, 1697 (molten)	k, 0.15 (molten)	~68	~120	(~30/**30**) 0	~29

Also, the analytically obtained cooling times showed excellent agreement with the numerical data. However, the reliability of this approach in some cases may be limited. An important drawback is that, if only the initial melt temperature (220 °C) is available for calculation, it will not be able to take into account the of effect injection time and therefore shear-heating. In other words, better estimation can be expected provided accurate melt temperature is available at the cross-section under consideration. However, it should be noted that the most prevalent parameter is the part thickness, any increment in thickness will cause quadratic rise in cooling time.

It may be stated that the most reliable estimations for cooling time are obtained by numerical simulations. Since present analyses consider cavity filling and cooling time estimation, more comprehensive information is obtained regarding heat transfer occurring during the injection cycle.
The cooling time in reality may be longer than the ones predicted by both numerical and analytical approaches. Although perfect contact between the part and mould surfaces are assumed, air gaps-acting as heat insulators-might develop between the solidifying part and mould wall surfaces, increasing the duration of required cooling time [21].

3.4. Importance of results in industrial application

The injection pressure, clamp force and cooling time obtained by simulations are of great importance for mould design and manufacturing considerations. With specific reference to pressure, this value can give an indication for geometrical constraints to be chosen for the gating system. As guidance for non-tapered cylindrical and strip gates, described by Equation 22-23 [23], the injection pressure is in direct proportion with the viscosity, L flow length, Q_{melt} volumetric flow rate and in inverse proportion with the R runner radius, strip w, h width and thickness respectively. Parameter n denotes the power-law index of the material.

$$P_{injection} \sim \frac{\eta L Q_{melt}^{n}}{R^{3n+1}} \qquad \text{Equation 22}$$

$$P_{injection} \sim \frac{\eta L Q_{melt}^{n}}{wh^{2n+1}} \qquad \text{Equation 23}$$

Since the apparent viscosity overestimated the injection pressure, this misleading information would lead the designer to reduce the injection pressure and associated pressure loss by increasing the diameter/thickness of the feed system.
Even though the true viscosity provided a more reliable estimation for the pressure, if the calculation is coupled with solid state heat capacity (regardless of whether solid or molten state thermal conductivity is used), the pressure and therefore the clamp force will be underestimated. The combination of this misleading information used for subsequent mould and process design may result in having a narrowed processing window, termination of manufacturing and/or financial loss.

According to Equation 22-23, increasing the dimension of the feed system may help to reduce the injection pressure and associated clamp force, however with specific reference to cooling time, increased gate radius/thickness increases the volume of the runner system, yielding longer cooling time, i.e. longer cycle time and more waste generated for cold runners [22].

Not only the injection pressure and clamp force would be underestimated by using the solid state heat capacity but the cooling time as well, with differences being dependent on whether solid or molten state thermal conductivity is used.
If underestimated cooling time is used for process design, sufficient part strength to retain the dimensional stability will not be accounted for and the part will deform upon ejection. On the other hand, if cooling time is estimated to be too long – and applied in reality – the part will be overcooled, leading to unnecessarily long cycle time and lower rate of productivity.

4. Conclusion

It has been shown that shear stress and rate corrections applied to the viscosity data have an impact on injection pressure prediction. When apparent viscosity was used for computation, the injection pressure was overestimated. For example, if the apparent viscosity was used, the definition for the radius of the runner system would be incorrectly interpreted. If the rheology measurements only permit the measurement of apparent viscosity, that may be used for quality assurance purposes and direct comparison of viscosity data. The most realistic prediction for injection pressure was obtained by using the true viscosity and molten state heat capacity, with thermal conductivity showing minor influence. Also, a sensitivity analysis to study the effect of NFT revealed that the adoption of NFT=T_g provided the most sensible estimation for injection pressure.
The most accurate prediction for cooling time was attained when both molten state heat capacity and thermal conductivity were utilised. Since the heat capacity and thermal conductivity are both the function of temperature, better approximations may be achieved if more data points are available for numerical computation. If reliable material data are available for simulations, improvements towards sustainable manufacturing can be achieved, i.e. cost savings and waste reduction might be realised.

5. Acknowledgements

The authors would like to acknowledge the support of the Advanced Sustainable Manufacturing Technologies (ASTUTE) project, which was part funded from the EU's European Regional Development Fund through the Welsh European Funding Office, in enabling the research upon which this paper is based. Further information on ASTUTE can be found at www.astutewales.com. The authors are also grateful for the technical support of MACH1 project at Swansea University.

6. References

[1] P. Kennedy, R. Zheng, Flow analysis of injection molds, Carl Hanser Verlag, ISBN 978-1-56990-512-8, Munich, 2013.
[2] M. Huszar, P. Wlodarski, F. Belblidia, S. Alston, C. Arnold, J. Sienz, D. Bould, The influence of apparent and true viscosity on injection pressure prediction, 23rd Conference on Computational Mechanics (ACME) Swansea, 2015.
[3] L.W. Seow, Y.C. Lam, Optimizing flow in plastic injection molding, Journal of Materials Processing Technology, 72 (1997) 333-341.
[4] H. Hassan, N. Regnier, G. Defaye, A 3D study on the effect of gate location on the cooling of polymer by injection molding, International Journal of Heat and Fluid Flow, 30 (2009) 1218-1229.
[5] A. Ozdemir, O. Uluer, A. Guldas, Flow front advancement of molten thermoplastic materials during filling stage of a mold cavity, Polymer Testing, 23 (2004) 957-966.
[6] M.C. Song, Z. Liu, M.J. Wang, T.M. Yu, D.Y. Zhao, Research on effects of injection process parameters on the molding process for ultra-thin wall plastic parts, Journal of Materials Processing Technology, 187-188 (2007) 668-671.
[7] T.V. Zhil`tsova, M.S.A. Oliveira, J.A.F. Ferreira, Relative influence of injection molding processing conditions on HDPE acetabular cups dimensional stability, Journal of Materials Processing Technology, 209 (2009) 3894-3904.
[8] R. Sánchez, J. Aisa, A. Martinez, D. Mercado, On the relationship between cooling setup and warpage in injection molding, Measurement, 45 (2012) 1051-1056.
[9] J.M. Dealy, J. Wang, Melt rheology and its applications in the plastics industry, Springer, ISBN 978-94-007-6394-4, Dordrecht, 2013.

[10] BS-ISO-11443, Plastics - Determination of the fluidity of plastics using capillary and slit-die rheometers, The BSI Standards Limited, 2014.
[11] G. Potsch, W. Michaeli, Injection molding, An introduction, Carl Hanser Verlag, ISBN-13: 978-1-56990-419-0, Munich, 2008.
[12] J. Aho, S. Syrjala, On the measurement and modeling of viscosity of polymer at low temperatures, Polymer Testing, 27 (2008) 35-40.
[13] Y.K. Shen, W.Y. Wu, An analysis of three-dimensional micro-injection molding, Int. Comm. Heat Mass Transfer, 29 (2002) 423-431.
[14] G.A. Mannella, V.L. Carrubba, V. Brucato, W. Zoetelief, G. Haagh, No-Flow Temperature in Injection Molding Simulation, Journal of Applied Polymer Science, 119 (2011) 3382-3392.
[15] B.L. Young, H.T. Kwon, K. Yoon, Numerical Prediction of Residual Stresses and Birefringence in Injection/Compression Molded Center-Gated Disk. Part I: Basic Modeling and Results for Injection Molding, Polymer Engineering and Science, 42 (2002) 2246-2272.
[16] A. Inc., Simulation Moldflow Insight, 2014.
[17] A.W. Birley, B. Haworth, J. Batchelor, Physics of plastics: processing, properties and materials engineering, Carl Hanser Verlag, ISBN 3-446-16274-7, Munchen, 1991.
[18] W.-H. Yang, A. Peng, L. Liu, D.C. Hsu, Integrated numerical simulation of injection molding using true 3D approach, SPE ANTEC (USA), 2004.
[19] G. Schramm, A practical approach to rheology and rheometry, Gebrueder HAAKE GmbH., Karlsruhe, 2000.
[20] H. Zhou, Computer modeling for injection molding: simulation, optimization and control, John Wiley & Sons Inc., ISBN 978-0-470-60299-72013.
[21] D.O. Kazmer, Injection mould design engineering, Hanser Gardner Publications Inc., ISBN-13: 978-1-56990-471-62007.
[22] R.A. Malloy, Plastic part design for injection molding, an introduction, Carl Hanser Verlag, ISBN-13: 978-1-56990-7, Munnich, 2010.
[23] J. Shoemaker, Moldflow Design Guide, Carl Hanser Verlag, ISBN-13: 978-1-56990-403-9, Munich, 2006.